

A Revised Mechanism for the Alkaline Phosphatase Reaction Involving Three Metal Ions

Boguslaw Stec¹, Kathleen M. Holtz² and Evan R. Kantrowitz^{2*}

¹Department of Biochemistry and Cell Biology, W. M. Keck Center for Computational Biology, Rice University Houston, TX 77005, USA

²Department of Chemistry Boston College, Chestnut Hill MA 02467, USA

Here, X-ray crystallography has been used to investigate the proposed double in-line displacement mechanism of *Escherichia coli* alkaline phosphatase in which two of the three active-site metal ions have a direct role in catalysis. Two new X-ray crystal structures of the wild-type enzyme in the absence and presence of inorganic phosphate have been refined at 1.75 Å to final working *R*-factors of 15.4% and 16.4%, respectively. In the refinement of both structures, residues in the active sites were treated anisotropically. The ellipsoids resulting from the partial anisotropic refinement show a clear route for the binding and release of substrate/product. In addition, a direct comparison of the refined structures with and without phosphate reveal a strong correlation between the occupancy of the third metal-binding site and the conformation of the Ser102 nucleophile. These findings clarify two important and unresolved aspects of the previously proposed catalytic mechanism, how Ser102 is activated for nucleophilic attack and why a magnesium ion in the third metal site is required for catalysis. Analysis of these results suggest that three metal-ion assisted catalysis is a more accurate description of the mechanism of the alkaline phosphatase reaction. A revised mechanism for the catalytic reaction of alkaline phosphatase is proposed on the basis of the two new X-ray crystal structures reported.

© 2000 Academic Press

Keywords: mechanism; catalysis; anisotropy; X-ray crystallography; phosphatase

*Corresponding author

Introduction

Alkaline phosphatase (E.C. 3.1.3.1) from *Escherichia coli* is a homodimeric enzyme that catalyzes the hydrolysis and transphosphorylation of a wide variety of phosphate monoesters. The enzymatic reaction proceeds through a covalent serine-phosphate intermediate to produce inorganic phosphate and an alcohol (Schwartz & Lipmann, 1961). Inorganic phosphate is also a strong competitive inhibitor of the enzyme and fills the entire volume of the shallow active-site pocket. Each active site of the dimeric enzyme contains three metal-binding sites (M1, M2 and M3). The M1 and M2 sites are occu-

piated by zinc ions (also referred to as Zn1 and Zn2), while the M3 site is occupied by a magnesium ion. The three metal ions in each active site form a catalytic metal triad similar to that of phospholipase C from *Bacillus cereus* (Hough *et al.*, 1989) and P1 nuclease from *Penicillium citrinum* (Volbeda *et al.*, 1991). In contrast to the two zinc ions, the magnesium ion in the M3 site has not been shown to play a direct role in catalysis, although it has been shown to be important for full enzyme activity (Anderson *et al.*, 1975; Xu & Kantrowitz, 1993; Tibbitts *et al.*, 1996).

X-ray crystallography has been used extensively in the study of *E. coli* alkaline phosphatase. The structure of the non-covalent product complex between the enzyme and inorganic phosphate (AP_1ALK, PDB entry 1ALK) has been determined to 2.0 Å and is the basis for the double in-line displacement mechanism of alkaline phosphatase involving two metal-ion assisted catalysis (Kim & Wyckoff, 1991). In the same study, a structure of the phosphate-free enzyme was determined to 2.8 Å resolution. Additional steps in the catalytic cycle have been determined from X-ray crystallo-

Abbreviations used: AP_1ALK, the structure of *Escherichia coli* alkaline phosphatase determined to 2.0 Å resolution (PDB code 1ALK); AP_noPi, the structure of *E. coli* alkaline phosphatase determined to 1.75 Å resolution reported here; AP_Pi, the structure of *E. coli* alkaline phosphatase determined to 1.75 Å resolution in the presence of phosphate reported here.

E-mail address of the corresponding author: evan.kantrowitz@bc.edu

graphy, including the covalent serine-phosphate intermediate captured in a crystal structure of the H331Q mutant enzyme (Murphy *et al.*, 1997) and a model of the proposed trigonal bipyramidal transition state determined in a crystal structure of the wild-type enzyme in the presence of vanadate (Murphy *et al.*, 1997). These structures further support the proposed catalytic mechanism (Kim & Wyckoff, 1991); however, important details of the mechanism remain unresolved. These include the mechanism by which the hydroxyl group of Ser102 is deprotonated for nucleophilic attack on the substrate, as well as the requirement for Mg in the third metal-binding site. The high-resolution X-ray crystal structures of alkaline phosphatase presented here provide answers to these questions and a revised catalytic mechanism for the reaction is proposed.

Results

Refinement and overall quality of the X-ray crystal structures

Based on the data collection and refinement statistics (see Table 1), the refined structures of alkaline phosphatase in the presence and absence of inorganic phosphate are improvements over the original determinations. The higher-resolution structures of this study provide a more accurate and detailed description of the entire molecule and especially the active site of the enzyme. The structures of alkaline phosphatase in the absence of phosphate (AP_noPi) and in the presence of phosphate (AP_Pi) were refined at 1.75 Å with final *R*-factors of 16.4% and 15.4%, respectively, based upon the data where $F_o/\sigma(F_o) > 4$. The R -factors using all the reflections were 19.6% for both structures. The final models included approximately 600 water molecules, corresponding to about 0.67 water molecule per amino acid residue. The refinement with SHELXL-97 (Sheldrick & Schneider, 1997), in full matrix mode, also allowed estimates in the coordinate errors to be determined for

individual atoms. The quality of the electron density maps are high in both structures, with only a few regions showing weaker electron density (three residues at the N termini that have weak backbone density, and a number of residues with weaker side-chain density, including 8, 252 to 253, 293 to 294, 357 to 358 and 407 to 408). The low crystallographic *R*-factor values, very good $2F_o - F_c$ electron density and the featureless $F_o - F_c$ difference electron density (± 0.28 electron/Å³) for both structures testify to the high fidelity of the refined models.

For the AP_Pi structure, the low RMSD of the backbone atoms between the A and B subunits (0.21 Å) is fully compatible with the expected error in individual atomic positions and is comparable to the RMSD between the A and B subunits of the AP_1ALK structure. The AP_Pi and AP_noPi structures are remarkably similar to each other and to the AP_1ALK structure (Kim & Wyckoff, 1991). The RMS deviation of backbone atoms between the AP_1ALK structure and the structures in this study was less than 0.22 Å.

The active sites of AP in the presence and absence of phosphate

The electron density for the active-site regions of both the AP_Pi and AP_noPi structures is shown in Figure 1. In the early stages of refinement, the difference Fourier maps clearly show the presence of inorganic phosphate in the active-site pocket of the structure of the AP_Pi complex and its absence in the AP_noPi structure. In the former structure, the occupancy of phosphate in each active site of the dimeric enzyme is 100%. In the AP_noPi structure, water molecules replace inorganic phosphate. The occupancies of these water molecules were difficult to establish, but have been formally refined to 100%. For these water molecules, a strong correlation is observed between small positional changes and the temperature/occupancy parameters. Nevertheless, reliable refinement of the temperature and occupancy parameters was possible with judicious use of BUMP constraints (0.1) in SHELXL-97 (Sheldrick & Schneider, 1997).

In the AP_Pi structure, the tetrahedral phosphate participates in interactions with the two active-site zinc ions, the guanidino nitrogen atoms of Arg166 and two water molecules. The bidentate interaction of Arg166 with the phosphate oxygen atoms is planar. The side-chain of Ser102 is clearly disordered, having two different conformations with occupancies of roughly 60 and 40%. In the major conformation, the Ser102 O^γ is within coordination distance to Zn2, 2.09 Å and 2.11 Å for the A and B subunits, respectively. In the major conformation, the side-chain of Ser102 also makes close contacts with the phosphate group. These close contacts indicate possible disorder in the phosphate position. Although not modeled, this disorder is detected in the anisotropic representation of the phosphate ion. In the minor conformation, the

Table 1. Refinement statistics

	AP_Pi	AP_noPi
Working <i>R</i> -factor		
4σ cutoff	0.154	0.164
All reflections	0.196	0.196
Free <i>R</i> -factor		
4σ cutoff	0.189	0.199
All reflections	0.235	0.236
Water molecules ^a	604	601
RMSD		
Bond lengths (Å)	0.018	0.019
Bond angles (Å)	0.034	0.037
Improper angles (deg.)	1.82	1.89
Dihedral angles (deg.)	24.7	24.8

^a Placement of final water molecules was done in SHELXL-97.

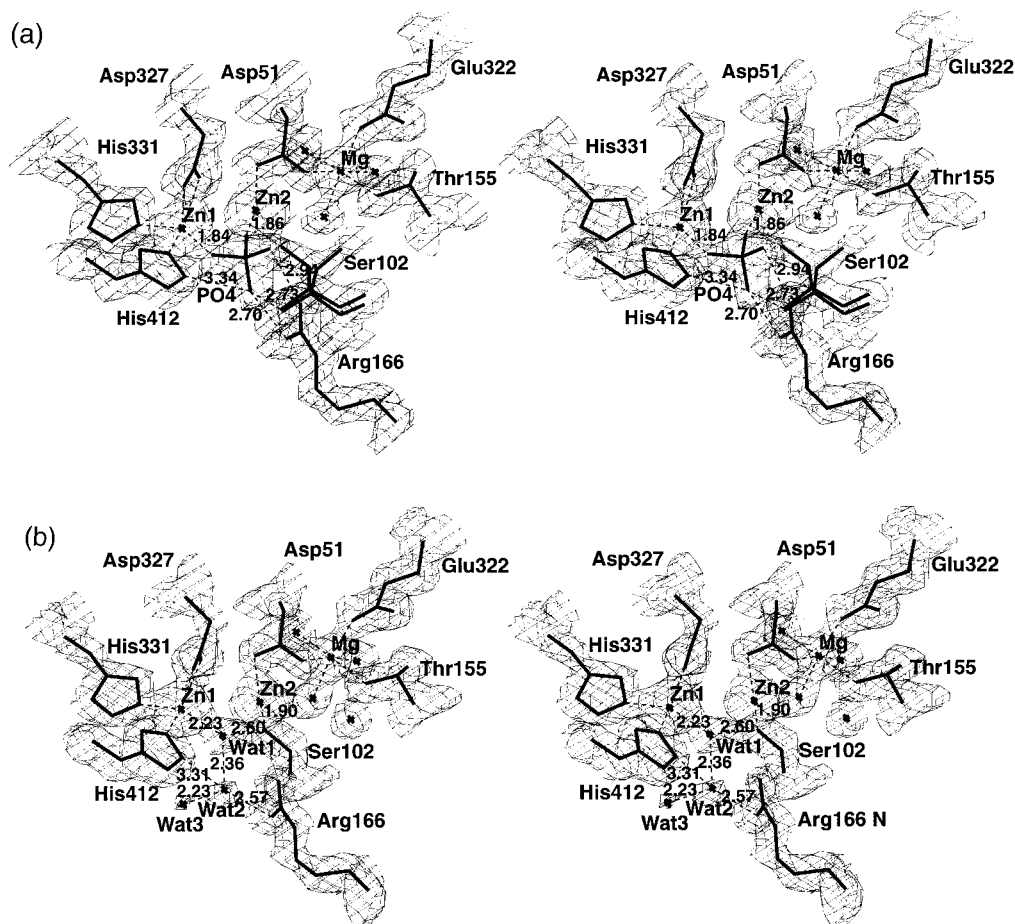


Figure 1. Stereoview of the $2F_o - F_c$ electron density maps ($\sigma = 1.5$) with the representative atomic model at the active sites of the (a) AP_Pi and (b) AP_noPi structures. The A subunit is shown.

side-chain of Ser102 displaces a water molecule and forms a hydrogen bond with the side-chain of Thr155. A summary of the enzyme-phosphate interactions and the corresponding distances is provided in Table 2.

In the AP_noPi structure, the active site contains three water molecules in place of inorganic phosphate and the side-chain of Ser102 is fully ordered. The hydroxyl group of Ser102 coordinates Zn2. The average distance between C γ of Ser102 and Zn2 of 1.91 Å suggests that the hydroxyl group is deprotonated. A water molecule bridges O γ of Ser102 and Zn1. This water molecule is the first in a short chain of three active-site water molecules. The second water molecule in this chain forms a hydrogen bond to a guanidino nitrogen atom (NH $_1$) of Arg166. The second guanidino nitrogen atom of Arg166 (NH $_2$) does not participate in hydrogen bonding to a water molecule. These water molecules are relatively close to each other, possibly suggesting that at least one is deprotonated and exists as a hydroxide ion (see Table 2).

Mg occupancy of the third metal-binding site in the AP_Pi and AP_noPi structures

Initially, the temperature factors for all three metal-binding sites in each active site of the AP_Pi structure were compared. The relatively low temperature factors for the Mg ions in the M3 site suggested that this metal-binding site contained a mixture of Mg and Zn ions. Partial occupancy by the heavier Zn ion lowers the temperature factor by dampening atomic vibrations. With SHELXL-97 (Sheldrick & Schneider, 1997) both metal ions were modeled into the same position at the M3 site in both the AP_Pi and the AP_noPi structures. Mixed occupancy was determined to be 60% Mg and 40% Zn in the AP_Pi structure. In the AP_noPi structure, the third metal-binding site appeared to be completely occupied by Mg. A negligibly small number, ~ 0.01 , was obtained for Zn occupancy of this site in the AP_noPi structure. The mixed occupancy of the M3 site in the AP_Pi structure was correlated with the observed disorder of the Ser102 side-chain in the same structure.

Table 2. Enzyme active-site interactions and distances

Structure	Interaction	Distance (Å) (ESD) ^a (subunit A/ subunit B)
AP_Pi	Zn2...O ₃ P	1.86(3)/1.89(3)
	Zn1...O ₂ P	1.84(3)/1.82(2)
	Zn2...O ^γ (Ser102)	2.09(6)/2.11(7)
	NH ₂ (Arg166)...O ₁ P	2.94(3)/2.85(4)
	NH ₁ (Arg166)...O ₄ P	2.70(3)/2.73(4)
	N(Ser102)...O ₄ P	2.73(3)/2.72(4)
	O ^{ε1} (His412)...O ₄ P	3.34(4)/3.20(4)
	Zn2...O ^γ (Ser102)	1.90(3)/1.93(4)
AP_noPi	C ^γ (Ser102)...Wat1	2.60(7)/2.64(6)
	Zn1...Wat1	2.23(6)/2.30(5)
	NH ₁ (Arg166)...Wat2	2.57(6)/2.63(6)
	N(Ser102)...Wat2	2.91(6)/2.99(6)
	C ^{ε1} (His412)...Wat2	3.31(7)/3.06(6)
	Wat1...Wat2	2.36(7)/2.23(6)
	Wat2...Wat3	2.23(7)/2.28(7)

^a Estimated standard deviations (ESD) are given in parentheses.

Anisotropic treatment of the active-site residues

In both structures, the active-site atoms have been refined with anisotropic temperature factors. After initial success in the anisotropic treatment of the metal cofactors, a second anisotropic refinement was attempted using approximately 210 active-site atoms with six thermal parameters. In order to achieve convergence, however, 204 and 171 active-site atoms were used in the anisotropic refinement of the AP_Pi and the AP_noPi structures, respectively. The anisotropy of these active-site atoms, with a maximum of approximately 4, varied as measured by the ratio of the major semi-axes. Atoms responsible for divergence showed negatively defined ellipsoids (i.e. a negative value for one of the semi-axes).

Despite difficulties in the refinement, the results represented by the major axis of the ellipsoids provide a clear sense of the direction of motion in the binding of substrate and the release of product. The direction of elongation for the active-site atoms and metal ions is in agreement with regard to the direction of motion of the substrate/product into and out of the active-site cavity. The path of motion is particularly evident from the anisotropic motion of Arg166. The major axis of the ellipsoid for Arg166 is perpendicular to the plane of the side-chain and approximately aligned with the elongated ellipsoids of the metal ions. This fact confirms a role for Arg166 in release of inorganic phosphate and possibly a role in the protonation of this ion. The anisotropic ellipsoids for the active-site atoms in the AP_Pi and the AP_noPi structures are shown in Figure 2.

The introduction of the anisotropic refinement step was validated by the behavior of the standard crystallographic *R*-factor as well as *R*_{free} (Figure 3). A direct comparison of the AP_noPi structure to the AP_Pi structure fully confirmed the increased mobility of the active site in the latter structure with more pronounced anisotropy for the metal

ions and the Arg166 side-chain in the presence of inorganic phosphate. An interesting observation is the elevated mobility observed for His331 and His412 in both structures.

Characterization of a sulfate-binding site

Based on the difference Fourier map, a sulfate-binding site is located in each subunit of both the AP_Pi and AP_noPi structures. This site, first identified by Tibbitts *et al.* (1994), is defined by residues in the region between 270 and 290. The occupancy of sulfate is lower in the B subunit in both structures of this study, suggesting that sulfate binding in the A subunit is greatly stabilized by an important crystal contact between the A subunit and the terminal lysine residue of a symmetry-related B subunit. This conclusion is supported by the lack of a sulfate-binding site in the structures of a series of alkaline phosphatase mutants at position 102, which crystallize in a different space group (Stec *et al.*, 1998). In both the AP_Pi and AP_noPi structures, an unusual conformation is detected for the backbone atoms of Asn293 in both subunits. This unusual conformation, characterized by backbone angles of $\Phi = 72^\circ$, $\Psi = 145^\circ$ in the AP_noPi structure and $\Phi = 102^\circ$, $\Psi = 140^\circ$ in the AP_Pi structure, is believed to be due to crystal contacts of the *I*222 space group and the formation of the sulfate-binding site.

Discussion

Two metal-ion assisted catalysis in alkaline phosphatase

The widely accepted two metal-ion assisted catalytic mechanism based on the structure described by Kim & Wyckoff (1991) (AP_1ALK) specifies the direct and important roles of Zn1 and Zn2 in the binding of substrate/product and in the formation of the nucleophiles. Zn2, in addition to substrate/

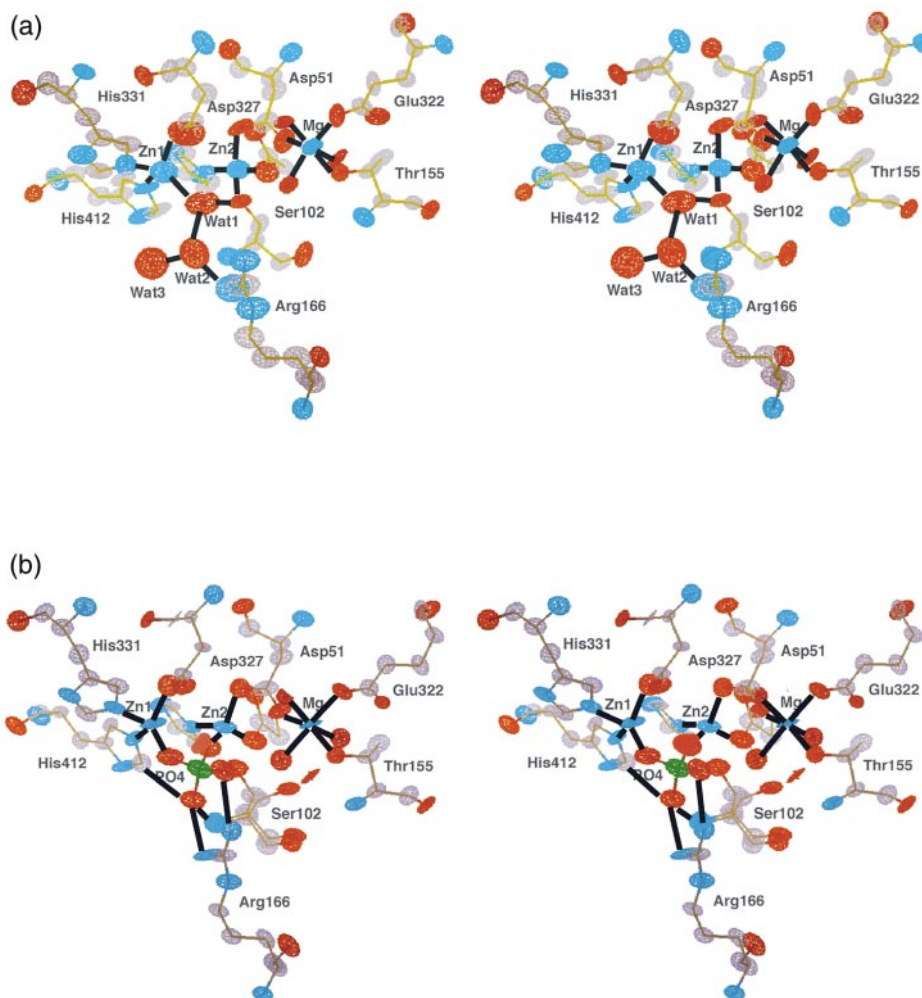


Figure 2. Stereoview of the anisotropic refinement of the active-site residues of the (a) AP_noPi and (b) AP_Pi structures. The atomic model with thermal ellipsoids represented at the 20% probability level is shown.

phosphate binding, coordinates the hydroxyl group of Ser102, activating it for nucleophilic attack on the phosphate monoester in the first step. Zn1 facilitates departure of the alcohol leaving group of the substrate in the first step, and then activates a water molecule for the second nucleophilic attack on the covalent serine-phosphate intermediate. Although the proposed catalytic mechanism is firmly established and well supported, several aspects remain unclear and have evaded detection in structural investigations. These include the mechanism by which the hydroxyl group of Ser102 is deprotonated for nucleophilic attack on the substrate, as well as the role of Mg and its requirement, as opposed to Zn, in the third metal-binding site. These questions are addressed below based upon a direct comparison of the two structures of the enzyme determined in this work.

Mg, in addition to Zn2, is required for Ser102 nucleophile generation

Based on the analysis of the AP_noPi and AP_Pi structures, Mg occupancy in the M3 metal-binding

site correlates with the conformation of the Ser102 side-chain. In the AP_noPi structure, exclusive Mg occupancy of the M3 site correlates with full coordination of the Ser102 side-chain to Zn2 as a deprotonated alkoxide ion. However, in the AP_Pi structure, the conformer placing Ser102 within coordination distance to Zn2 (60% occupancy) correlates with 60% occupancy of Mg in the M3 binding site. Conversely, Zn bound in the M3 site of this structure (40% occupancy) agrees well with the side-chain conformer of Ser102 with 40% occupancy rotated away from the phosphate-binding pocket and Zn2. The strong correlation between the M3 metal ion and the Ser102 side-chain conformer in the AP_Pi structure suggests that Mg is required for deprotonation of the hydroxyl group of the nucleophile.

Proton abstraction from the Ser102 hydroxyl group requires a general base. The octahedral Mg ion in the M3 site is coordinated by the side-chain oxygen atoms of Asp51, Thr155 and Glu322, and three water molecules. One of the water molecules is in close proximity to Zn2 (4.7 Å) and the side-chain hydroxyl group of Ser102 (3.1 Å). Based on

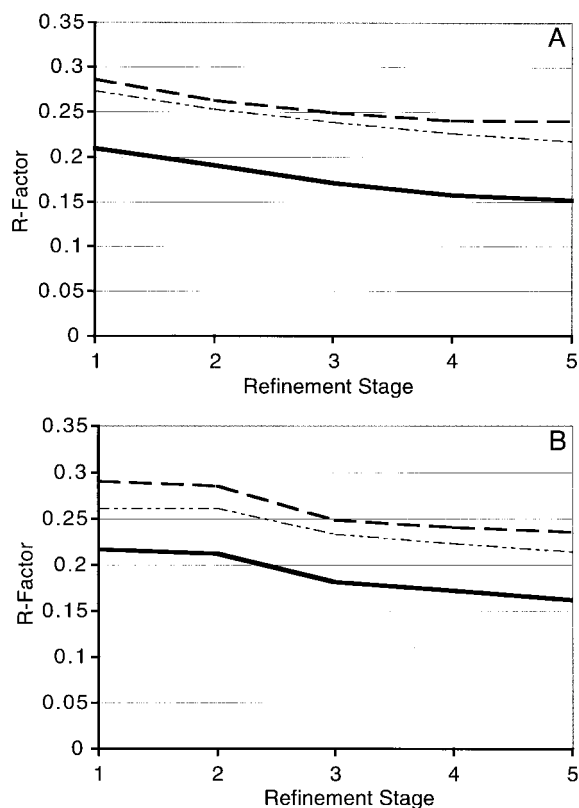


Figure 3. The behavior of the R_{σ} (continuous line), R_{FREE} (broken line) and R_{ALL} (dash-dot-dot) at different stages of the refinement with SHELXL-97 (Sheldrick & Schneider, 1997) for the (a) AP_Pi and (b) AP_noPi structures. The five refinement stages are: (1) protein alone; (2) protein, metals and phosphate; (3) protein, metals, phosphate and 50% of the water molecules; (4) protein, metals, phosphate and all the water molecules; and (5) protein, metals, phosphate, waters plus an isotropic refinement of the active-site atoms.

the short oxygen to Mg distance (2.10 Å, average distance in both structures), this water molecule may be coordinated as a hydroxide ion. A Mg-coordinated hydroxide ion could function as a general base and accept the proton from O^{γ} of the Ser102 side-chain. Following this proton transfer, O^{γ} of Ser102 is stabilized by coordination to Zn2. Based upon a comparison of the AP_Pi and AP_noPi structures presented here, a specific role for Mg is proposed in the generation of the Ser102 nucleophile.

The octahedral coordination geometry of Mg in the M3 binding site is required for Ser102 deprotonation

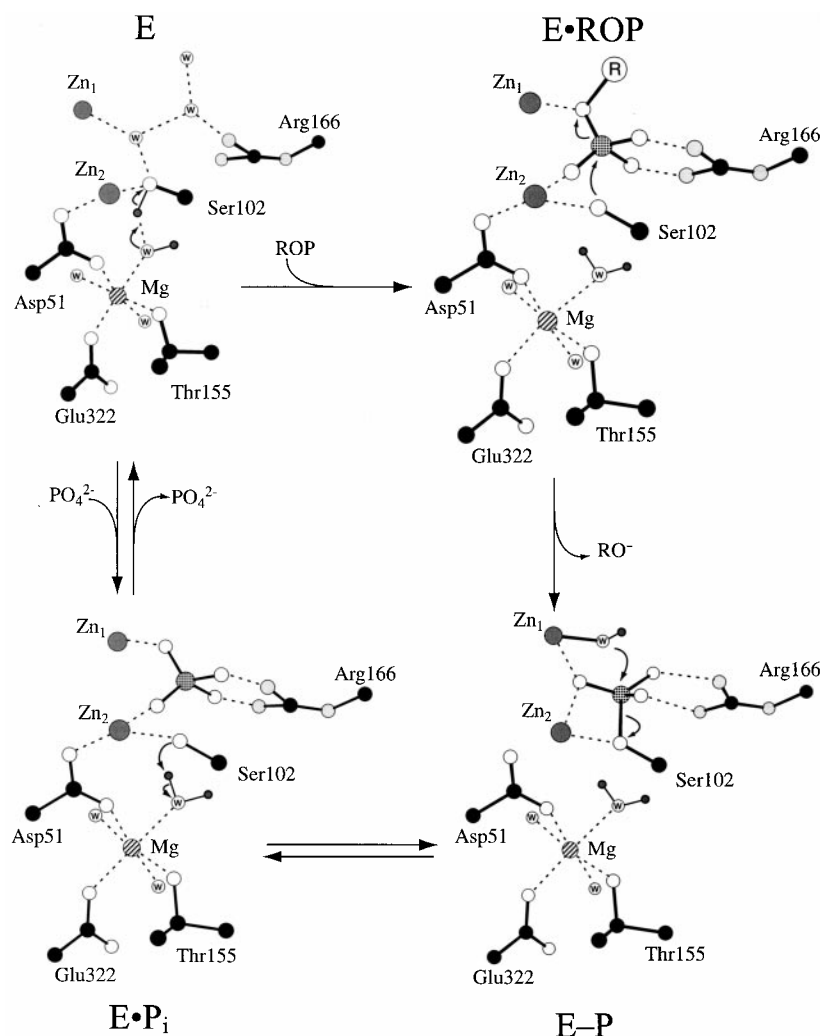
The requirement of a magnesium ion in the M3 site for maximal activity has not been fully understood, despite considerable efforts (Xu & Kantrowitz, 1993; Murphy *et al.*, 1993, 1995; Tibbitts *et al.*, 1996). Based on the AP_Pi and

AP_noPi structures and in agreement with other work, the metal ion in the M3 site appears to directly influence catalysis through its coordination geometry. The octahedral coordination sphere of Mg in the M3 site is necessary to optimally position the proton-accepting hydroxide ligand. Although not directly observed from the electron density maps, the binding of a third Zn ion in the M3 site (as observed in 40% occupancy of the AP_Pi structure) may change the octahedral coordination sphere into a tetrahedral one. Both Zn1 and Zn2 have tetrahedral geometries in alkaline phosphatase. If Zn-binding in the M3 site does not disrupt the octahedral geometry, its smaller ionic radius may distort the spatial arrangement of the six ligands. In either case, the metal-bound hydroxide group serving as a general base is likely to be shifted from its optimal position. Consequently, the Ser102 side-chain cannot form a hydrogen bond with the metal-associated hydroxide group, and is rotated away from the Zn2 ion in the conformer that has 40% occupancy in the AP_Pi structure.

The importance of the geometry of the metal ion in the M3 site on catalysis is observed in a mutant version of alkaline phosphatase. Based on the X-ray structure of this single-site mutant, the octahedral Mg-binding site is converted into a distorted, tetrahedral Zn-binding site, thereby reducing the activity of this enzyme drastically in the absence of exogenous magnesium (Murphy *et al.*, 1993, 1995). The mechanistic details elucidated in this study provide a rationale for the requisite octahedral geometry of Mg in the M3 site.

A revised catalytic mechanism for alkaline phosphate: three metal-ion catalysis

The mechanism for alkaline phosphatase proposed (Figure 4) here builds upon that originally proposed by Kim & Wyckoff (1991). In the free enzyme (E, Figure 4, top left), three water molecules fill the active site and the Ser102 hydroxyl group participates in a hydrogen bond with the Mg-coordinated hydroxide ion. Upon binding of the phosphomonoester (ROP) to form the Michaelis enzyme-substrate complex (E·ROP, Figure 4, top right), the Ser102 O^{γ} becomes fully deprotonated for nucleophilic attack with the concomitant transfer of the proton to the Mg-coordinated hydroxide group to form a Mg-coordinated water molecule. Coordination of Zn2 stabilizes Ser102 O^{γ} in its nucleophilic state. In the first in-line displacement, the activated hydroxyl group of Ser102 attacks the phosphorus center of the substrate in the enzyme-substrate complex (E·ROP) to form a covalent serine-phosphate intermediate (E-P, Figure 4, bottom right). Zn1 participates in this step by coordinating the bridging oxygen atom of the substrate and facilitating the departure of the alcohol leaving group (RO^{-}). In the second in-line displacement step, a nucleophilic hydroxide ion coordinated to Zn1 attacks the phosphorus atom, hydrolyzing the



covalent serine-phosphate intermediate to form the non-covalent enzyme-phosphate product complex (E·P_i, Figure 4, bottom left) and regenerate the nucleophilic Ser102. Zn₁ lowers the pK_a of the coordinated water molecule to effectively form the nucleophilic hydroxide ion, while the Mg-coordinated water molecule acts as a general acid to reprotonate O^γ of Ser102. Protonation of Ser102 may facilitate departure of the phosphate product from the non-covalent E·P_i complex. Alternatively, the Mg-coordinated water molecule may directly protonate the phosphate group for its release. The release of phosphate from the E·P_i complex to give the free enzyme (E, Figure 4, top left) may be facilitated also by the increased mobility of the Arg166 side-chain.

Conclusion

The in-depth crystallographic investigation of the AP_{Pi} and AP_{noPi} structures reported here suggests that the mechanism of the alkaline phosphatase reaction involves three metal-ion assisted

Figure 4. The catalytic mechanism of alkaline phosphatase. Hydrogen atoms have been included only at catalytically relevant sites. In the free enzyme (E), the phosphate-binding site is filled with three water molecules. The Ser102 hydroxyl group participates in a hydrogen bond with a Mg-coordinated hydroxide ion. Formation of the enzyme-substrate complex (E·ROP) involves coordination of the ester oxygen atom to Zn₁ and additional interactions between the non-bridging oxygen atoms of the substrate with Zn₂ and the guanidinium group of Arg166. Ser102 occupies the position opposite the leaving group. Upon phosphomonoester binding, the Mg-coordinated hydroxide ion acting as the general base deprotonates Ser102 O^γ for nucleophilic attack on the phosphorus atom. The formation of the covalent enzyme-phosphate intermediate (E·P) results in inversion of the phosphorus center and the loss of the leaving group (RO⁻). A nucleophilic hydroxide ion coordinated to Zn₁ attacks the covalent E·P intermediate, forming the non-covalent enzyme-phosphate complex (E·P_i) and causing a second inversion of configuration at the phosphorus center. The water molecule coordinated to Mg now acts as a general acid, donating a proton to O^γ of Ser102 or, alternatively, inorganic phosphate. Most of the hydrogen atoms and ligands to Zn₁ and Zn₂ are not shown.

catalysis. This three metal-ion mechanism proposed for alkaline phosphatase can be related directly to a whole class of enzyme mechanisms involving three metal ions, such as that observed in phospholipase C (Hough *et al.*, 1989). For the first time, this study offers evidence for a direct role of the Mg ion, the third metal ion of the catalytic triad, in the mechanism. The Mg occupancy-dependence of the M3 site on the Ser102 conformation strongly implicates a well-positioned, Mg-bound water molecule as the general base in the generation of the Ser102 nucleophile, and as a general acid in the regeneration of the Ser102 hydroxyl group. The octahedral geometry established by a Mg ion in the M3 site is necessary to position the water molecule for its function. In addition to elucidating the mechanism of primary nucleophile activation, these structures provide a visual understanding of the movement of substrate and product in and out of the active site, through the use of anisotropic temperature factors in the refinement.

Materials and Methods

Materials

Agar, agarose, ampicillin, *p*-nitrophenylphosphate, magnesium chloride, and zinc chloride were purchased from Sigma Chemical Co. Tris, sucrose, and enzyme-grade ammonium sulfate were supplied by ICN Bio-medicals. Tryptone and yeast extract were obtained from Difco Laboratories.

Strains

The Δ *phoA* *Escherichia coli* K12 strain SM547 [Δ (*phoA-phoC*), *phoR*, *tsx::Tn5*, Δ *lac*, *galK*, *galU*, *leu*, *str^r*] was a gift from H. Inouye.

Methods

Purification of the alkaline phosphatase

E. coli alkaline phosphatase was isolated as described (Chaidaroglou *et al.*, 1988). *E. coli* SM547 cells transformed with the plasmid pEK48 was used as the host strain for expression of wild-type alkaline phosphatase. The concentration of purified enzyme was determined from absorbance measurements at 280 nm using an extinction coefficient of 0.71 cm² mg⁻¹ (Plocke & Vallee, 1962).

Crystallization and preparation of phosphate-free AP crystals

Wild-type alkaline phosphatase was crystallized by vapor diffusion using hanging drops of 15 μ l. The enzyme solution, at approximately 30 mg/ml, was first dialyzed against a 20% saturated solution of (NH₄)₂SO₄ in 100 mM Tris (pH 9.5), 10 mM MgCl₂, 0.01 mM ZnCl₂. Crystals formed in reservoirs with the ammonium sulfate concentration between 39% and 43% saturated. Crystals were transferred into stabilizing solution containing 55% saturated (NH₄)₂SO₄, 100 mM Tris (pH 7.5), 10 mM MgCl₂, 1 mM ZnCl₂. For the preparation of phosphate-free crystals, the stabilization solution contained 1 M Tris and was exchanged several times prior to the data collection. Stopped-flow kinetics on enzyme solutions dialyzed in 1 M Tris shows that the buffer completely removes inorganic phosphate from the enzyme.

X-ray data collection

Crystals having approximate dimensions of 1.0 mm \times 0.6 mm \times 0.4 mm were mounted into glass capillaries. The diffraction data were collected at room temperature using two multiwire area detectors (Area Detector Systems, San Diego, CA), driven by a VAX ALPHA 3300 computer and linked to Rigaku RU-200 rotating-anode generator operated at 50 kV and 150 mA using the Crystallographic Facility in the Chemistry Department of Boston College. Diffraction data for both crystals with and without phosphate were collected at 1.75 Å resolution. The data collection statistics are summarized in Table 3. For the AP_Pi structure, a total of 116,956 unique reflections were obtained from measurements with an average redundancy of 3.0 (Table 3). For the AP_noPi structure, a total of 116,126 unique reflections were obtained from measurements with an average redundancy of 3.3 (Table 3). Merging of the reflections was accomplished using the software provided by Area

Detector Systems. After correction for Lorentz and polarization effects, a scale factor was calculated for multiple measurements and symmetry-related reflections.

Modeling and structural refinement

The initial model used for the refinement of the AP_Pi and the AP_noPi structures was the coordinates of *E. coli* alkaline phosphatase determination to 2.0 Å resolution (AP_1ALK) (PDB code 1ALK), with phosphate and water molecules removed. X-PLOR (Brünger, 1992) and IMPLOR (Polyvision, Inc. Hopedale, MA) were used initially to refine the coordinates. Based upon the initial electron density of the (2F_o - F_c) and (F_o - F_c) maps for the AP_Pi structure, phosphate was bound in the active site of the enzyme. In the AP_noPi structure, water molecules were present in the active site in place of phosphate. In the second round of refinement, water ligands to the metal ions were included in both structures. Both structures were further refined by positional refinement, temperature factor refinement, and simulated annealing. Positional and temperature factor refinement improved working and free R-factors initially. Each refinement cycle was finished with visual inspection of the model and manual rebuilding, if necessary. Only a few residues from the original model required repositioning. The refinements were carried out using Silicon Graphics Indigo II computers. An automated water placement feature of IMPLOR was used to add solvent water molecules based on the difference Fourier map (F_o - F_c), their distance from surrounding residues, and their temperature factors.

In the final stages of refinement, SHELXL-97 was used to refine the structures (Figure 3). Explicit hydrogen atoms were introduced into the structures after the first round of refinement with SHELXL-97 in order to improve the goodness of fit parameter and the quality of the resulting electron density maps. After convergence was reached, the temperature factors for the active-site residues and metal cofactors were refined anisotropically. Initially, only the metal cofactors were refined with anisotropic temperature factors, then residues of the active site were included. In the AP_noPi structure, 204 active-site atoms were treated anisotropically. In the AP_Pi structure, only 171 atoms could be treated anisotropically, probably reflecting the higher R_{merge} for this data set (6.4%) compared to the data set for the phosphate-free enzyme (6.3%). When 204 active-site atoms are treated anisotropically in the AP_Pi structure, the

Table 3. Data collection summary

Structure	AP_Pi	AP_noPi
Space group	<i>I</i> ₂₂₂	<i>I</i> ₂₂₂
<i>d</i> _{min} (Å)	1.75	1.75
Reflections unique	116,956	116,126
<i>I</i> / σ (<i>I</i>)	10.3	14.4
Last shell (1.75-1.82 Å)	1.4	1.4
Completeness (%)	92.6	92.0
Last shell (1.75-1.82 Å)	74.5	75.1
Average redundancy	3.0	3.3
Last shell (1.75-1.82 Å)	1.81	1.76
Unit cell (Å)	<i>a</i> =195.11 <i>b</i> =167.31 <i>c</i> =76.81	<i>a</i> =195.37 <i>b</i> =167.69 <i>c</i> =76.43
Final R _{merge} ^a	0.064	0.063

$$^a R_{\text{merge}} = \frac{\sum_{hkl} \sum_i |I_{\text{mean}} - I_i|}{\sum_{hkl} \sum_i I_i}$$

refinement showed divergence (non-positive definite matrix) and much stronger restraints would have been required to reach convergence (Murshudov *et al.*, 1999).

Acknowledgments

This work was supported by the National Institutes of General Medical Sciences (GM48233). B.S. acknowledges partial support from the Keck Center for Computational Biology.

References

- Anderson, R. A., Bosron, W. F., Kennedy, F. S. & Vallee, B. L. (1975). The role of magnesium in *Escherichia coli* alkaline phosphatase. *Proc. Natl Acad. Sci. USA*, **72**, 2989-2993.
- Brünger, A. T. (1992). *X-PLOR Version 3.1: A system for X-ray Crystallography and NMR*, Yale University Press, New Haven, CT.
- Chaidaroglou, A., Brezinski, J. D., Middleton, S. A. & Kantrowitz, E. R. (1988). Function of arginine in the active site of *Escherichia coli* alkaline phosphatase. *Biochemistry*, **27**, 8338-8343.
- Hough, E., Hansen, L. K., Birknes, B., Jynge, K., Hansen, S., Hordvik, A., Little, C., Dodson, E. J. & Derewenda, Z. (1989). High-resolution (1.5 Å) crystal structure of phospholipase C from *Bacillus cereus*. *Nature*, **338**, 357-360.
- Kim, E. E. & Wyckoff, H. W. (1991). Reaction mechanism of alkaline phosphatase based on crystal structures two metal-ion catalysis. *J. Mol. Biol.* **218**, 449-464.
- Murphy, J. E., Xu, X. & Kantrowitz, E. R. (1993). Conversion of a magnesium binding site into a zinc binding site by a single amino acid substitution *Escherichia coli* alkaline phosphatase. *J. Biol. Chem.* **268**, 21497-21500.
- Murphy, J. E., Tibbitts, T. T. & Kantrowitz, E. R. (1995). Mutations at positions 153 and 328 in *Escherichia coli* alkaline phosphatase provide insight towards the structure and function of mammalian and yeast alkaline phosphatases. *J. Mol. Biol.* **253**, 604-617.
- Murphy, J. E., Stec, B., Ma, L. & Kantrowitz, E. R. (1997). Trapping and visualization of covalent enzyme-phosphate intermediate. *Nature Struct. Biol.* **4**, 618-621.
- Murshudov, G. N., Vagin, A. A., Lebedev, A., Wilson, K. S. & Dodson, E. J. (1999). Efficient anisotropic refinement of macromolecular structures using FFT. *Acta Crystallog. sect. D*, **55**, 247-255.
- Plocke, D. J. & Vallee, B. L. (1962). Interaction of alkaline phosphatase of *E. coli* with metal ions and chelating agents. *Biochemistry*, **1**, 1039-1043.
- Schwartz, J. H. & Lipmann, F. (1961). Phosphate incorporation into alkaline phosphatase of *E. coli*. *Proc. Natl Acad. Sci. USA*, **47**, 1996-2005.
- Sheldrick, G. M. & Schneider, T. R. (1997). High-resolution refinement. *Methods Enzymol.* **277**, 319-343.
- Stec, B., Hehir, M. J., Brennan, C., Nolte, M. & Kantrowitz, E. R. (1998). Kinetic and X-ray structural studies of three mutant *E. coli* alkaline phosphatases: insights into the catalytic mechanism without the nucleophile Ser102. *J. Mol. Biol.* **277**, 647-662.
- Tibbitts, T. T., Xu, X. & Kantrowitz, E. R. (1994). Kinetics and crystal structure of a mutant *Escherichia coli* alkaline phosphatase (Asp-369 → Asn): a mechanism involving one zinc per active site. *Protein Sci.* **3**, 2005-2014.
- Tibbitts, T. T., Murphy, J. E. & Kantrowitz, E. R. (1996). Kinetic and structural consequences of replacing the aspartate bridge by asparagine in the catalytic metal triad of *Escherichia coli* alkaline phosphatase. *J. Mol. Biol.* **257**, 700-715.
- Volbeda, A., Lahm, A., Sakiyama, F. & Suck, D. (1991). Crystal structure of *Penicillium citrinum* P1 nuclease at 2.8 Å resolution. *EMBO J.* **10**, 1607-1618.
- Xu, X. & Kantrowitz, E. R. (1993). Binding of magnesium in a mutant *Escherichia coli* alkaline phosphatase changes the rate-determining step in the reaction mechanism. *Biochemistry*, **32**, 10683-10691.

Edited by R. Huber

(Received 21 January 2000; received in revised form 13 April 2000; accepted 13 April 2000)